Fabrication and Characterization of Large Macroporous Photonic Crystals in Titania

Judith E. G. J. Wijnhoven,† Lydia Bechger, and Willem L. Vos*

van der Waals-Zeeman Instituut,‡ Universiteit van Amsterdam, Valckenierstraat 65, NL-1018 XE Amsterdam, The Netherlands

Received June 25, 2001. Revised Manuscript Received September 3, 2001

We made large, highly ordered structures consisting of crystals of macropores in titania (TiO_2), by template-assisted growth. The crystals were characterized by synchrotron small-angle X-ray diffraction, X-ray absorption, wide-angle X-ray diffraction, scanning electron microscopy, optical microscopy, optical reflectivity, and Raman spectroscopy. Care was taken to make well-ordered templates, by slowly growing colloidal crystals from lightly charged polystyrene latex particles and carefully drying them to form opals. Solid material was deposited in the opal template by precipitation from an alkoxide hydrolysis. Subsequently, the samples were heated to 450 °C to form anatase TiO_2 and to remove the latex template, which resulted in a macroporous crystal, inverse opal, or air-sphere crystal. The macropores were close-packed and interconnected by windows, and small additional voids were located at interstices between the pores. The macropores were arranged on a face-centered cubic lattice with domains of more than 750 × 350 × 250 unit cells. The size polydispersity of the air spheres and mean-squared displacements from the lattice sites were studied for the first time. Both quantities were small, thus quantifying the excellent long-range order. The lattice parameter was shrunk by about 30% relative to the template, irrespective of the radii of the pores, while the long-range order persisted. The surfaces of the macropores appeared to be rough up to length scales of ∼10 nm, the sizes of the largest TiO_2 crystallites, with a roughness distribution following a power law. The volume fraction of the solid backbone was determined for the first time in situ by X-ray absorption and was found to be between 5 and 12 vol % TiO_2. The wavelengths of the optical Bragg reflections were proportional to the radii of the air spheres. By the use of the measured TiO_2 fraction, the refractive index of the solid matrix was found to be 2.7 ± 0.4, in good agreement with the refractive index of massive anatase TiO_2. We briefly explored the assembly of macropores in rutile-TiO_2 and in rock salt. It was concluded that macroporous crystals are highly effective three-dimensional photonic crystals.

Introduction

The development of porous materials is a subject of intensive research. Well-known structures such as zeolites are widely used in everyday life. Recently, macroporous materials, that is, materials with pores with radii larger than 25 nm, have been under intense scrutiny for their great potential in novel applications in separation science, catalysis, and in particular photonic materials. There are several different approaches to realize structures with the desired length scales. Macroporous materials can be made by etching voids or channels in massive materials, such as semiconductors.[1,2] The complementary technique of template-assisted assembly of macroporous materials is undergoing rapid development.[3−22]

In template-assisted growth, a template is made by the self-assembly of bacteria,[6] emulsions,[7] colloidal suspensions,[8−17] or block copolymers.[18] As a next step,

* To whom correspondence should be addressed. E-mail: wvos@science.uva.nl.

† Present address: van 't Hoff Laboratorium, Universiteit Utrecht, Padualaan 8, 3584 CH Utrecht, The Netherlands.

‡ URL: www.photonicbandgaps.com.

(1) Grüning, U.; Lehmann, V.; Ottow, S.; Busch, K. *Appl. Phys. Lett.* **1996**, *68*, 747−749.

(2) Schuurmans, F. J. P.; Vanmaekelbergh, D.; van de Lagemaat, J.; Lagendijk, A. *Science* **1999**, *284*, 141−143.

(3) Velev, O. D.; Kaler, E. W. *Adv. Mater.* **2000**, *12*, 531−534.

(4) Xia, Y.; Gates, B.; Yin, Y.; Lu Y. *Adv. Mater.* **2000**, *12*, 693−713.

(5) Norris, D. J.; Vlasov, Y. A. *Adv. Mater.* **2001**, *13*, 371−376.

(6) Davis, S. A.; Burkett, S. L.; Mendelson, N. H.; Mann, S. *Nature* **1997**, *385*, 420−423.

(7) Imhof, A.; Pine, D. J. *Nature* **1997**, *389*, 948−951.

(8) Velev, O. D.; Jede, T. A.; Lobo, R. F.; Lenhoff, A. M. *Nature* **1997**, *389*, 447−448.

(9) Antonietti, M.; Berton, B.; Göltner, C.; Hentze, H. P. *Adv. Mater.* **1998**, *10*, 154−159.

(10) Holland, B. T.; Blanford, C. F.; Stein, A. *Science* **1998**, *281*, 538−540.

(11) Wijnhoven, J. E. G. J.; Vos, W. L. *Science* **1998**, *281*, 802−804.

(12) Yang, P.; Deng, T.; Zhao, D.; Feng, P.; Pine, D.; Chmelka, B. F.; Whitesides, G. M.; Stucky, G. D. *Science* **1998**, *282*, 2244−2246.

(13) Velev, O. D.; Jede, T. A.; Lobo, R. F.; Lenhoff, A. M. *Chem. Mater.* **1998**, *10*, 3597−3602.

(14) Holland, B. T.; Blanford, C. F.; Do, T.; Stein, A. *Chem. Mater.* **1999**, *11*, 795−805.

(15) Yin, J. S.; Wang, Z. L. *Adv. Mater.* **1999**, *11*, 469−472.

(16) Zakhidov, A. A.; Baughman, R. H.; Iqbal, Z.; Cui, C.; Khayrullin, I.; Dantas, S. O.; Marti, J.; Ralchenko, V. G. *Science* **1998**, *282*, 897−901.

10.1021/cm0111581 CCC: $20.00
Published on Web 12/17/2001

the solid material is grown between the template by the use of, e.g., a chemical reaction in which a precipitate is formed. Other methods which can be used to infiltrate a template are filling with a saturated solution of a salt, a melt, a suspension of nanoparticles that settle between the template, sol−gels, or chemical vapor deposition.[3−21] Finally, the template is removed by etching or calcination and the porous material remains. Until now, this method has already lead to a host of different macroporous materials such as ceramics,[6−15] carbon,[16] semiconductors,[17,19,20] and polymers.[18,21] See also refs 3, 4, and 5 for recent reviews of this rapidly developing field.

It has become widely recognized that macroporous materials are important candidates for photonic crystals.[22] Photonic crystals are three-dimensional periodic dielectric composites with lattice parameters on the order of the wavelength of light.[23,24] Photonic crystals are especially pursued to achieve photonic band gaps that allow the control of spontaneous emission and the localization of photons.[25,26] A photonic band gap can be described in simple terms as a band of wavelengths that are Bragg diffracted in all directions simultaneously. There are several important requirements for photonic crystals.

First, to operate at optical wavelengths, the lattice parameter of the crystal must be on the order of several tenths of micrometers to several micrometers. Colloidal particles are very well-suited as building blocks for templates because they are readily available with the desired range in sizes; they can be made with a small size variation and they spontaneously form crystals with long-range order.[27,28] The alternative name of inverse opals for ordered macroporous crystals is also en vogue since templates made of dried colloidal crystal are artificial opals.

Second, the refractive index ratio between the air in the macropores and the solid backbone should be high, while optical absorption should be as low as possible. It appears that titania is a well-suited material because it combines a high refractive index (about 2.6 at 500 nm wavelength for anatase[29]) with a large electronic band gap of 3 eV and it can be made with high purity. This is confirmed by the widespread use of titania by many groups, see refs 10, 14, and 30−33.

Third, the macropores should be very well-ordered on a lattice, because photonic effects are based on optical Bragg diffraction phenomena from crystal lattice planes. For the ubiquitous face-centered cubic (fcc) structure formed by colloids,[27,28] the photonic band gap will occur in the frequency range of second-order Bragg diffraction.[34,35,36] It is well-known that high-order diffraction is much more sensitive to disorder than the first-order diffraction,[37] which is also borne out by recent calculations.[38] Thus, much effort should be invested in making a good template, since the macroporous material is an imprint of that template.

In this paper, we describe methods to fabricate well-ordered macroporous photonic crystals in anatase titania that are successfully used in optical experiments[36,39−44] and we explore alternative methods to make samples from rutile and rocksalt. We analyze our samples with many different methods, including small-angle X-ray scattering (SAXS) techniques[45] that appear to be new to macroporous materials and well-known methods such as scanning electron microscopy (SEM), optical microscopy, wide-angle X-ray diffraction, and optical reflectivity. Scattering techniques are excellent complementary techniques to imaging methods such as microscopy. The latter provide detailed local information about the geometry and morphology of the inverse opals and allow study of characteristic defects. Scattering methods are sensitive to long-range order of the crystal and statistical averages.[45,37] Therefore, for the first time, we can address the size polydispersity and surface roughness of the pores in macroporous crystals. Since X-rays penetrate the whole sample, SAXS provides information about ordering in the bulk and not only of the surface as with electron microscopy. SAXS is a nondestructive analysis; the sample can be used afterward, e.g., for optical experiments. For electron microscopy, the samples had to be sputtered with gold before analysis, which renders them useless for optical experiments. Moreover, the vacuum in an electron microscope can also damage the samples.[46] We use SAXS as

(17) Vlasov, Y. A.; Yao, N.; Norris, D. J. *Adv. Mater.* **1999**, *11*, 165−168.
(18) Jenekhe, S. A.; Chen, X. L. *Science* **1999**, *283*, 372−375.
(19) Braun, P. V.; Wiltzius, P. *Nature* **1999**, *402*, 603−604.
(20) Blanco, A.; Chomski, E.; Grabtchak, S.; Ibisate, M.; John, S.; Leonard, S. W.; Lopez, C.; Meseguer, F.; Miguez, H.; Mondia, J. P.; Onzin, G. A.; Toader, O.; van Driel, H. M. *Nature* **2000**, *405*, 437−440.
(21) Park, S. H.; Xia, Y. *Adv. Mater.* **1998** *10*, 1045.
(22) Jacoby, M. *Chem. Eng. News* **1998**, *76*, 38−43.
(23) *Photonic Band Gap Materials*; Soukoulis, C. M., Ed.; Kluwer Academic Press: Dordrecht, The Netherlands, 1996.
(24) *Photonic Crystals and Light Localization in the 21st Century*; Soukoulis, C. M., Ed.; Kluwer Academic Press: Dordrecht, The Netherlands, 2001.
(25) Yablonovitch, E. *Phys. Rev. Lett.* **1987**, *58*, 2058−2061.
(26) John, S. *Phys. Rev. Lett.* **1987**, *58*, 2486−2489.
(27) Vos, W. L.; Megens, M.; van Kats, C. M.; Bösecke, P. *Langmuir* **1997**, *13*, 6004−6008.
(28) Megens, M.; van Kats, C. M.; Bösecke, P.; Vos, W. L. *J. Appl. Crystallogr.* **1997**, *30*, 637−641.
(29) *Landolt-Börnstein, Zahlenwerte und funktionen, Optische Konstanten*; Bartels, J., Ed.; Springer: Berlin, 1962 (II. Band, 8. Teil). We have isotropically averaged the ordinary and extraordinary refractive indices of TiO_2, which is a birefringent material.
(30) Subramania, G.; Constant, K.; Biswas, R.; Sigalas, M. M.; Ho, K.-M. *Appl. Phys. Lett.* **1999**, *74*, 3933−3935.
(31) Subramanian, G.; Manoharan, V. N.; Thorne, J. D.; Pine, D. J. *Adv. Mater.* **1999**, *11*, 1261−1265.
(32) Richel, A.; Johnson, N. P.; McComb, D. W. *Appl. Phys. Lett.* **2000**, *76*, 1816−1818; **2000**, *77*, 1062−1063.
(33) Rengarajan, R.; Jiang, P.; Colvin, V.; Mittleman, D. *Appl. Phys. Lett.* **2000**, *77*, 3522−3519.
(34) Sözüer, H. S.; Haus, J. W.; Inguva, R. *Phys. Rev. B* **1992**, *45*, 13962−13972.
(35) Busch, K.; John, S. *Phys. Rev. E* **1998**, *58*, 3896−3908.
(36) Vos, W. L.; van Driel, H. M. *Phys. Lett. A* **2000**, *272*, 101−106.
(37) Guinier, A. *X-ray diffraction*; Dover Publication Inc.: New York, 1994.
(38) Li, Z. Y.; Zhang, Z. Q. *Phys. Rev. B* **2000**, *62*, 1516−1519.
(39) Thijssen, M. S.; Sprik, R.; Wijnhoven, J. E. G. J.; Megens, M.; Narayanan, T.; Lagendijk, A.; Vos, W. L. *Phys. Rev. Lett.* **1999**, *83*, 2730−2733.
(40) van Driel, H. M.; Vos, W. L. *Phys. Rev. B* **2000**, *62*, 9872−9875.
(41) Koenderink, A. F.; Megens, M.; van Soest, G.; Vos W. L.; Lagendijk, A. *Phys. Lett. A* **2000**, *268*, 104−111.
(42) Schriemer, H. P.; van Driel, H. M.; Koenderink, A. F.; Vos, W. L. *Phys. Rev. A* **2001**, *63*, 011801.
(43) Vos, W. L.; van Driel, H. M.; Megens, M.; Koenderink, A. F.; Imhof, A. In *Photonic Crystals and Light Localization in the 21st Century*; Soukoulis, C. M., Ed.; Kluwer Academic Press: Dordrecht, The Netherlands, 2001; pp 191−218.
(44) Koenderink, A. F.; Bechger, L.; Schriemer, H. P.; Lagendijk, A.; Vos, W. L. To be published.
(45) Feigin, L. A.; Svergun, D. I. *Structure Analysis by Small-Angle X-ray and Neutron Scattering*; Plenum: New York, 1987.
(46) Jiang, P.; Bertone, J. F.; Hwang, K. S.; Colvin, V. L. *Chem. Mater.* **1999**, *11*, 2132−2140.

Table 1. Radii of Particles in Opal Templates, Radii of Air Spheres, Shrinkage of Air-Sphere Crystals, Volume Fraction of Solids in Opal Templates, and Volume Fractions of Matrixes in Filled Opals and in Air-Sphere Crystals[a]

template		inverse opals						volume fractions		
R_1 (nm)	δ (%)	R_{SEM} (nm)	R_{SAXS1} (nm)	R_{SAXS2} (nm)	R_{SEM} (nm)	R_{SAXS1} (nm)	R_{SAXS2} (nm)	φ_{opal} (%)	φ_{filled} (%)	$\varphi_{titania}$ (%)
180	1.5	173 ± 3	164 ± 4	178.6 ± 0.3	118 ± 3	127 ± 4	127 ± 4	75		
213	2.0	226 ± 2			148 ± 3				>4.9	6.6
241	1.0	250 ± 8	240 ± 4	243.9 ± 0.1	187 ± 10	170 ± 4 to 178 ± 3	183 ± 1 to 194 ± 2	91	>4.9	5−7.6
261	2.1	258 ± 4			177 ± 2					
326	1.9	322 ± 3								
426	1.4				300 ± 3					11.7
439	1.4	463 ± 2	436 ± 9	438.6 ± 0.2	325 ± 5 to 344 ± 5	304 ± 5	307 ± 1	75	>4.3	8.3−10.6
1460 TiO_2	2.8	1480 ± 5			988 ± 22					
1460 NaCl	2.8	1480 ± 5			1494 ± 11					

[a] R_1 is radius as given by the supplier, δ is size polydispersity as given by the supplier, R_{SEM} is radius determined from SEM images, R_{SAXS1} is radius obtained from the lattice parameter determined by X-ray scattering, R_{SAXS2} is radius calculated from the X-ray formfactor measurements, and φ is volume fraction of solid material obtained from X-ray absorption measurements.

opposed to light scattering, since photonic crystals modify the well-known Bragg diffraction law[47] and since a large range of length scales can be probed, as demonstrated with colloidal photonic crystals.[27] Advantages of SAXS over neutron scattering are the excellent beam collimation and monochromaticity. Using X-ray absorption experiments, we study, for the first time, in situ the volume fraction of solid material, which is an essential parameter for the theoretical interpretation of optical data, e.g., with photonic band structure calculations. From optical reflectivity experiments, we infer the optical properties of the solid backbone of the structure.

Experimental Section

To grow templates, we used 10 vol % colloidal suspensions of polystyrene latex spheres in water, as obtained from the supplier (Duke Scientific), with radii R and small size polydispersities listed in Table 1. The suspensions were sealed in flat glass capillaries (Vitro Dynamics, dimensions of 100 × 3 × 0.3 mm^3). Colloidal crystals were grown by sedimentation; a thin layer of crystals was first nucleated in a centrifuge. Subsequently, each capillary was left to stand still for up to 2 months, until the suspension had completely sedimented and crystallized (in the case of suspensions with R > 400 nm). Crystals of spheres with R < 400 nm were grown within a day in a centrifuge. After the suspensions had completely crystallized, the top of each capillary was opened. The water above and in the crystals was slowly evaporated over a time of about 1−2 months. This process resulted in artificial opals of latex spheres.

To infiltrate the interstitial space of the opals with TiO_2, we used liquid precursors consisting of mixtures of titanium(IV) propoxide (TPT, 98%, Aldrich) and ethanol, in proportions ranging from 20 to 100 vol % TPT. Occasionally, we used other precursors: titanium(IV) isopropoxide (TiPT) and titanium(IV) ethoxide (TET). The capillaries containing the opals were opened at the bottom and placed inside a nitrogen-purged glovebox in a small bottle that contained the liquid precursor. The liquid entered the opals and filled the voids between the spheres by capillary forces. Typically, infiltration of an opal takes about $^1/_2$ h. After infiltration, the opals were taken out of the glovebox to let the precursor react with water from the air for about a day. The cycle of infiltration, reaction, and drying was repeated 1−8 times depending on the concentration TPT in the ethanol. When a capillary did not get filled anymore within 2−3 h, no more infiltrations were attempted. To obtain inverse opals of NaCl, we infiltrated the template with a hot saturated NaCl solution. The samples were then left to cool and dry.

After infiltrating the opals, the samples were heated in an oven in air. In a typical heating procedure, the temperature was increased at a rate of 5 °C h^{-1}, stabilized at 80 °C for 1 h, further heated, and stabilized at 450 °C for 6 h before being decreased to ambient temperature at a rate of 10 °C h^{-1}.

The samples were characterized by optical microscopy, SEM, SAXS, and X-ray absorption. Optical microscope photos were taken with an Olympus SZ60 microscope, equipped with an Olympus SC35-12 camera. The SEM images were taken with an ISI DS-130 scanning electron microscope, after sputtering the samples with a thin layer of gold. Some of the samples were tilted in the direction of the detector to get a better signal. Corrections for the tilt were taken into account for the measurement of the sphere sizes from the images.

SAXS and X-ray absorption experiments were performed at beamline 4/ID2 of the European Synchrotron Radiation Facility (ESRF).[48] The incident beam was monochromatic with a wavelength of $\lambda = 0.098\,950\,6$ nm and a relative bandwidth of $\Delta\lambda/\lambda = 1.5 \times 10^{-4}$. The beam was focused to a narrow spot of about 0.3 × 0.6 mm with a maximum beam flux of 10^{13} photons/s. Both the incident flux and the transmitted flux were monitored with PIN diodes. The samples were mounted on two translation stages that scanned the spatial position with respect to the horizontal X-ray beam and a rotation stage that scanned about the vertical axis (ω-axis). The samples were aligned such that the flat faces were perpendicular to the incident beam at $\omega = 0°$. The radiation scattered by the sample was detected with a CCD camera equipped with a fluorescent screen that was placed at a distance of 10 m from the sample. The smallest observable scattering vector $s = 2\sin(\theta)/\lambda$ is $s_{min} = 1.8 \times 10^{-3}$ nm^{-1}, with 2θ the diffraction angle. The resolving power Δs is better than 4×10^{-4} nm^{-1}.

Wide-angle X-ray diffraction was done on a Nonius PDS120 powder diffractometer equipped with a CPS120 detector, using a Cu Kα generator at a wavelength of $\lambda = 0.154$ nm. The volume-averaged grain sizes were calculated from the diffraction peak broadening using Scherrer's equation.[37]

Results and Discussion

(1) Templates and Infiltration. (a) Opal Templates. Figure 1a shows an optical micrograph of two samples of opal templates made of spheres with R = 439 nm. The bright colors are optical Bragg diffractions from the crystal planes. Different colors appear because the angle of incidence of the illuminating white source varies with respect to the crystal planes. Moreover, the

(47) Vos, W. L.; Sprik, R.; van Blaaderen, A.; Imhof, A.; Lagendijk, A.; Wegdam, G. H. *Phys. Rev. B* **1996**, *53*, 16231−16235; **1997**, *55*, 1903 (erratum).

(48) Bösecke, P.; Diat, O. *J. Appl. Crystallogr.* **1997**, *30*, 867−871.

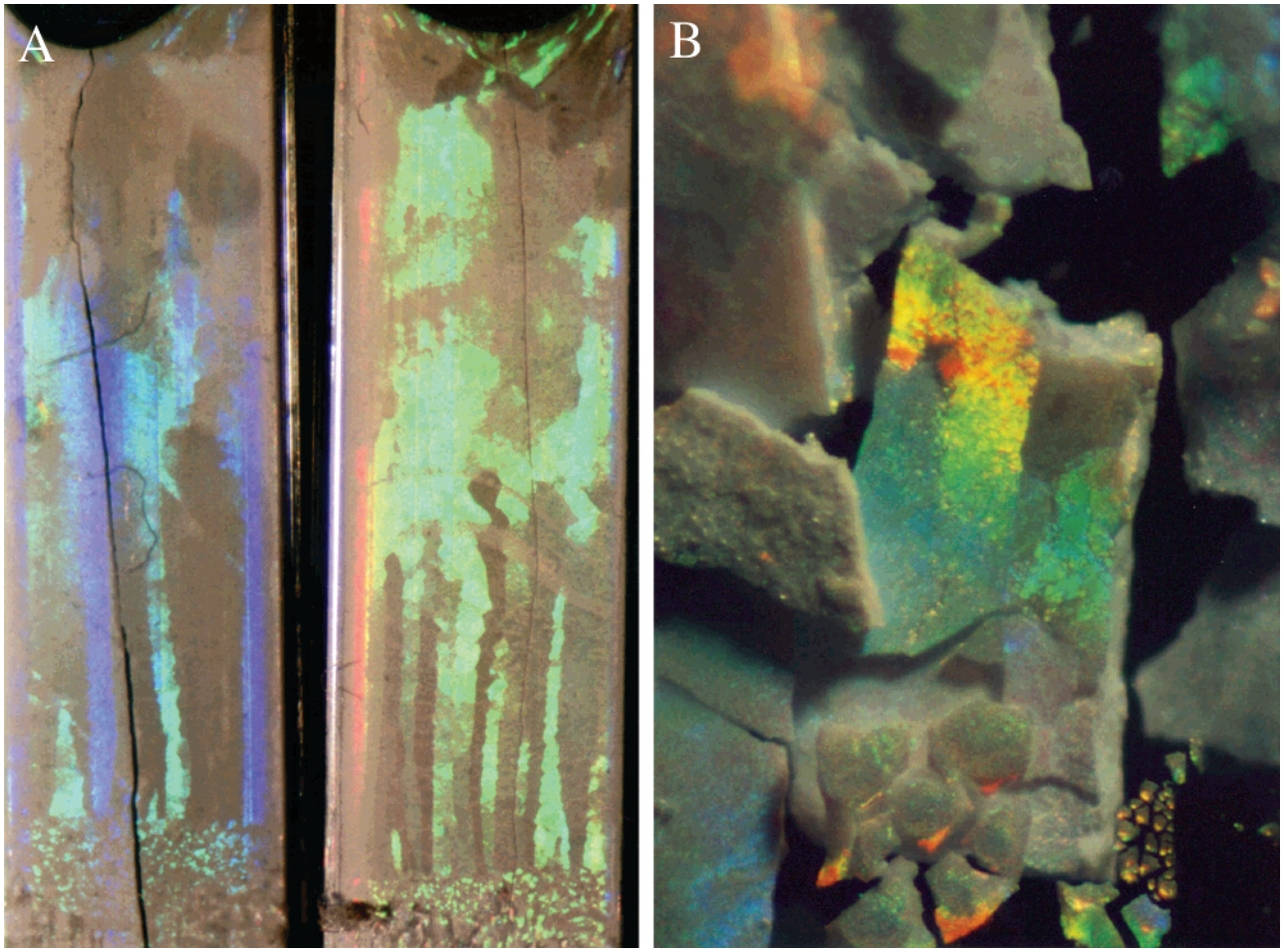

Figure 1. (a) Optical micrograph of two opals made of latex spheres with radii of 439 nm. The width of the capillaries in which the opals are grown is 3 mm. The blue and green colors are optical Bragg reflections. The upper parts of the samples consist of large crystals, due to slow sedimentation. At the bottom of both capillaries, many small crystallites are visible as a result of fast crystallization by centrifugation. (b) Optical micrograph of an inverse opal in titania (pore radius = 305 nm) made of a template as shown in Figure 1a. The size of this crystal is about 1 mm^2. The crystals show similar long colored bands as the opal that served as the template. The appearance of several colors is due to high-order multiple Bragg diffraction.[36,40]

colors correspond to high-order Bragg diffraction, since the lattice parameter $a = 1240$ nm is large compared to the wavelengths of visible light ($\lambda = 400-750$ nm) and different high-order diffraction conditions are easily met for slightly different angles of observation. The difference between slow and fast crystallization can clearly be seen in Figure 1a; the crystals grown in a centrifuge, in the lower part in the capillary, show many glittering spots, whereas slowly grown crystals show long colored bands from the top to the bottom of the capillary. These bands are very long single-domain crystals, up to 1 cm; the spots are small crystallites, up to 150 μm. It will be confirmed below that the crystals with the large domains are the best templates for inverse opals.

Once a colloidal crystal has been formed in suspension, the drying should be done very carefully because the initial colloidal crystal has a volume fraction of 50−60%[27] and the remaining opal consists of up to 74% of polystyrene spheres.[49] Due to the densification, the opal develops fissures, apparent as a vertical line in each sample in Figure 1a. The green sample on the right shows the common case of a fissure that tracks grain boundaries on the edges of the colored bands and hardly damages the large domains.

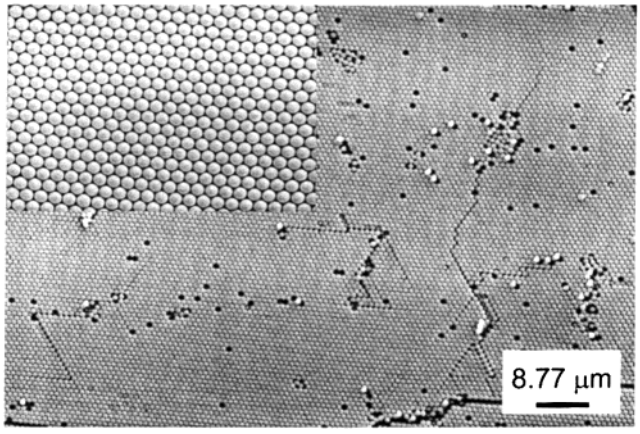

Figure 2. Inset: SEM image of opal template (particle radius $R = 463 \pm 2$ nm). The spheres are well-ordered in a hexagonal plane, i.e., the fcc [111] plane. Main: zoomed-out SEM image of a different part of the same sample. Vacancies are attributed to the removal of the opal from the capillary, and line defects are attributed to drying or to the vacuum of the SEM.

Figure 2 shows SEM images of the surfaces of an opal template with $R = 439$ nm. The inset of Figure 2 shows a close-up of a perfect region which is 18 × 24 spheres

(49) Ashcroft, N. W.; Mermin, N. D. *Solid State Physics*; W. B. Saunders Company: New York, 1976.

large, that is, 15 × 20 μm. The arrangement of spheres shows the typical hexagonal close-packed (hcp) plane corresponding to fcc [111] planes[27] that preferentially grow parallel to glass walls of containers. A factor that most likely contributes to the perfection of colloidal crystals is the use of particles with a small size polydispersity ΔR, in this case, a size variation as small as $\Delta R/R = 1.4\%$.

Figure 2 shows an overview of a different part of the same sample. Inside this large well-ordered single crystal of 98 × 127 spheres (86 × 112 μm), we notice several vacancies and line defects. The vacancies in the surface are most likely not intrinsic to the crystal or limitations in crystal growth but they are attributed to the removal of the opal from its capillary; spheres may stick to the capillary wall thereby leaving vacancies in the opal. Indeed, a number of such spheres are visible on the surface of the opal and all spheres are displaced to the left of the created vacancies. Several line defects are seen, for instance, at the right from the center. Nevertheless, they are relatively small and do not disrupt the size of this large crystal domain.

In the lower right of Figure 2, a fissure is seen. It is attributed either to shrinkage during drying, also suggested by Park and Xia,[50] or to shrinkage in the vacuum of the SEM as proposed by Jiang et al.[46] The orientation of the crystal below this defect is the same as above, and the edges of the domains above and below the fault fit together like pieces of a jigsaw puzzle. Similar breaks are also observed in opals grown by other methods.[46,50] Jiang et al. report cracks at every 10 μm in most of their thin-film samples.[46] The larger distance of several hundred micrometers observed in our samples is tentatively ascribed to the greater thickness of our samples. In optical experiments, such fault lines will be likely to result in diffuse scattering that reduces the apparent reflectivity or transmission[39,40] This scattering may contribute to enhanced backscattering.[41] Large domains with at least 100 units in each direction, such as the one in Figure 2, are expected to reveal photonic crystal properties close to the theoretical limit of large crystals.[23,24]

In Table 1, the first five columns list the radii and polydispersities of the latex spheres that we used, as given by the supplier and as determined from SEM and SAXS. The sizes of the latex colloids agree very well with the sizes given by the supplier, except for the spheres with a radius specified as 213 nm that have a radius of 225 ± 3 nm. The excellent agreement was also observed earlier on smaller polystyrene particles.[51]

(b) Infiltration. We obtained the best infiltration results with TPT as the precursor. TPT itself is quite viscous, and it does not fill the opal well. By the mixing of TPT with ethanol, the viscosity is lowered and the wetting properties are possibly improved because the mixtures infiltrate the opal quite well. On the other hand, the concentration of TPT should be high enough, otherwise many infiltration cycles become necessary. During the infiltration, the lower part of the capillary is filled in the best manner, and the best samples are usually obtained from this part. The upper part of the capillary will be filled relatively incompletely due to the fact that the space between the spheres gets blocked by the titania in the lower part. As a result, the volume fraction of TPT is the lowest at the top of the capillary. A possible remedy is to add precursor from the top of the capillary. In our experience, a mixture of 50 vol % of both components appeared to be optimal.

We also used other precursors such as TiPT and TET. TiPT is much less viscous than TPT. It can even be used in pure form, but it does not seem to give better crystals. We observed that TET does not fill the templates well. For our infiltration method, TPT turned out to be the most suitable precursor. An extensive study of various alkoxides has been performed by Holland et al.[14] In this paper, TET is used as precursor for the synthesis of TiO_2. The cause of the difference between the results of Holland et al. and our experience is tentatively attributed to the fact that Holland et al. used a different infiltration method; an opal template is placed on a filter, the liquid is poured on the opal, and the vacuum below the filter draws the liquid into the opal in addition to the capillary forces that are the only forces in our infiltration method.

Another interesting approach of infiltration is to combine the template formation with the infiltration, as has been done by Subramania et al.,[30] Subramanian et al.,[31] and Vaudreuil et al.[52] The former two groups mixed colloidal spheres for the template with a slurry of nanocrystalline titania for the infiltration, and the latter suspended the colloidal spheres in an alkoxide solution. While Subramania et al.[30] obtain distorted crystals and Vaudreuil et al.[52] did not observe crystallization, Subramanian et al.[31] reported well-ordered samples.

(c) Calcination. The infiltrated opal is heated to remove the latex by gasifying and burning. Heating is also necessary to complete the reaction of the alkoxides to solid TiO_2. Indeed, Raman spectra of the infiltrated but not yet calcinated opals revealed complicated spectra that are very different from any known polymorph of titania (e.g., ref 11). It is surmised that in this stage, the solid is a complex conglomerate that contains many hydroxy and alkoxy groups.

Figure 3 shows a sequence of wide-angle X-ray diffraction patterns taken from TPT, which has reacted in the absence of opals with water from the air and which was heated to three final temperatures. After 10 h at 250 °C, no diffraction peaks are apparent at all. Heating for 7 h at 350 °C gives one weak peak suggesting that crystallization of anatase has started. Heating for 5 h at 450 °C yields a diffraction pattern with many diffraction peaks that agrees very well with the anatase form of titania. The averaged grain size of the particles is found to be 20.2 ± 1.2 nm. A high-resolution diffraction pattern of an inverse opal measured on ID 9 of the ESRF revealed 16 diffraction peaks that could all be matched with anatase TiO_2 reflections up to $hkl = 415$. This pattern attests to the purity of the material, since we estimate the upper bound on non-anatase TiO_2 phases such as rutile, Brookite, or "Grey-titania" to be less than 1%.

(50) Park, S. H.; Xia, Y. *Langmuir* **1999**, *15*, 266−273.
(51) Megens, M.; van Kats, C. M.; Bösecke, P.; Vos, W. L. *Langmuir* **1997**, *13*, 6120−6129.
(52) Vaudreuil, S.; Bousmina, M.; Kaliaguine, S.; Bonneviot, L. Presented at the International Symposium on Mesoporous Molecular Sieves, Québec City, Canada, Aug 27−Sept 2, 2000.

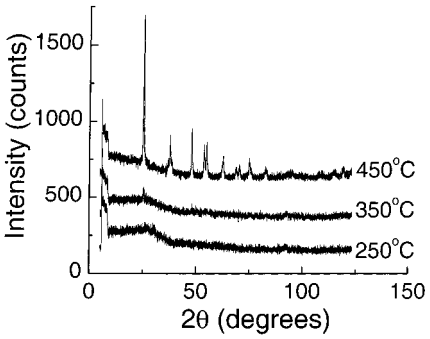

Figure 3. Wide-angle X-ray diffraction patterns of reacted TPT. For the lower pattern, the middle curve, and the upper curve, the material has been heated to 250, 350, and 450 °C, respectively. The lower pattern shows no diffraction peaks, the middle pattern shows a weak peak at the position of the strongest anatase diffraction peak ($2\theta = 25.3°$), and the upper diffraction pattern is in excellent agreement with the anatase diffraction pattern.

Since the inverse opals are composed of small titania particles, the samples are expected to reveal optical Rayleigh scattering, i.e., the well-known scattering from particles that are much smaller than the wavelength of light. If the titania inverse opals are viewed in directions away from optical Bragg reflections, they appear white as shown in Figure 1b, because the many particles in a sample give rise to multiple scattering. The whiteness of the materials, in conjunction with long light paths that are manifest in enhanced backscattering experiments,[41] is evidence for low optical absorption and concomitant material purity. In ref 43, a large absorption length of more than 10^5 wavelengths is deduced.

Recently, we let the TPT-infiltrated opals react with an excess of water instead of water from the atmosphere. We observed partial crystallinity at lower temperatures of 350 °C when compared to the reaction without added water, and after heating to 450 °C, the grain sizes were smaller. It seems that this method yields inverse opals with somewhat better ordered structures over the earlier reactions without added water. The proposed reason is that the crystallization of TiO_2 has already started at a lower temperature while the template is still present[53] and the crystallization is thus structurally better controlled.

Alternatively, if TPT reacts in an acidic environment, i.e., in the presence of 1% v/v nitric acid (65%), some diffraction peaks can be seen even at 250 °C. After heating to 450 °C, these crystallites are smaller compared to the reaction in a neutral environment. Clearly, different reaction conditions lead to a variation in crystallization temperature and grain size.

Thermogravimetric analysis (TGA) experiments by Yan et al.[53] have revealed that all latex is removed at a temperature of 350 °C. Thus, the temperature of 450 °C that is used to complete the reaction to anatase TiO_2 is certainly sufficient to remove the template and obtain inverse opals. The observation of fully crystallized anatase at 450 °C agrees well with TGA experiments that reveal an exothermic peak at 404 °C.[54]

(53) Yan, H. W.; Blanford, C. F.; Holland, B. T.; Smyrl, W. H.; Stein, A. *Chem. Mater.* **2000**, *12*, 1134−1141.

(54) Zhou, Q.; Wu, S.; Zhang, Q.; Zhang, J.; Chen, J.; Zhang, W. *Chin. Phys. Lett.* **1997**, 14, 306−309.

As an alternative to heating, we also extracted the latex with an organic solvent, tetrahydrofuran. This yielded a disordered inverse structure without long-range order, and the sample broke into small pieces. These results are attributed to a swelling of the polystyrene particles before their dissolution. By the dissolution of the polystyrene, the sample does not get heated; therefore, the reaction to crystalline TiO_2 does not get completed.

(2) Inverse Opals. (a) Optical Microscopy. Figure 1b shows an optical micrograph of inverse opal with pore radii $R_{SAXS1} = 304$ nm that was prepared from colloids with radii $R = 439$ nm (see Table 1). The bright colors are optical Bragg diffractions, as with the parent opals (cf. Figure 1a). In passing, we note that for the inverse opals, the high-order diffraction appears to be a complex multiple diffraction phenomenon that completely modifies the usual diffraction conditions.[36] Figure 1b shows that after calcination, the samples break up into pieces up to a few millimeters in size. This is sufficiently large to perform various optical experiments to probe photonic crystal effects, see refs 36, and 39−42. The pieces consist of several single-crystal domains, containing at least 700 × 350 × 250 unit cells; see the section on SAXS below. Centrifuged samples, the ones with $R < 400$ nm, also form millimeter-sized grains, albeit consisting of smaller domains (see refs 39, 41, and 42). The breaks between the particles seem to occur preferentially along grain boundaries between the large domains. Grain boundaries between the domains can be seen in the inverse opals in Figure 1b and are similar to features in the parent opal. Thus, inverse opals also mirror the structure of the parent opals on a macroscopic scale.

(b) SEM. Parts a−f of Figure 4 show SEM images of inverse opals. Figure 4a shows the surface of a sample with macropore radii $R_{SAXS1} = 304$ nm, made with extra water during the synthesis. The macropores, or air spheres, form a nearly perfect hexagonal arrangement of 12 × 14 spheres, or 7.3 × 8.5 μm, corresponding to a [111] plane of the fcc structure. In our experience, the flat surfaces of the crystals (cf. Figure 1b) are invariably the [111] planes, because upon crystallizing the template, the colloids prefer to order themselves parallel to the capillary wall.[27,28] The highly ordered structure of macropores confirms that inverse opals are faithful replicas of the original opal templates (cf. inset of Figure 2).

The inset of Figure 4a shows a rarely observed cleavage: a [110] plane. The macropores are arranged in typical rectangles with edges with ratios of 1 to $2^{1/2}$. The small holes between the air spheres are macropores from a crystal plane that is sitting on top of the plane containing the large pores; the pores of the top plane have been cut off at a peculiar height, i.e., not halfway through the macropore diameter, as with the [111] plane, to form shallow holes.

The dark spots indicated with arrows in Figure 4a are the connections between the macropores and the nearest-neighbor pores in the layer below, called windows. The windows correspond to points where the latex spheres in the template were touching each other. The precursors or the reaction products do not cover the colloidal spheres in areas centered at those places, probably for reasons of diffusion or wetting. After

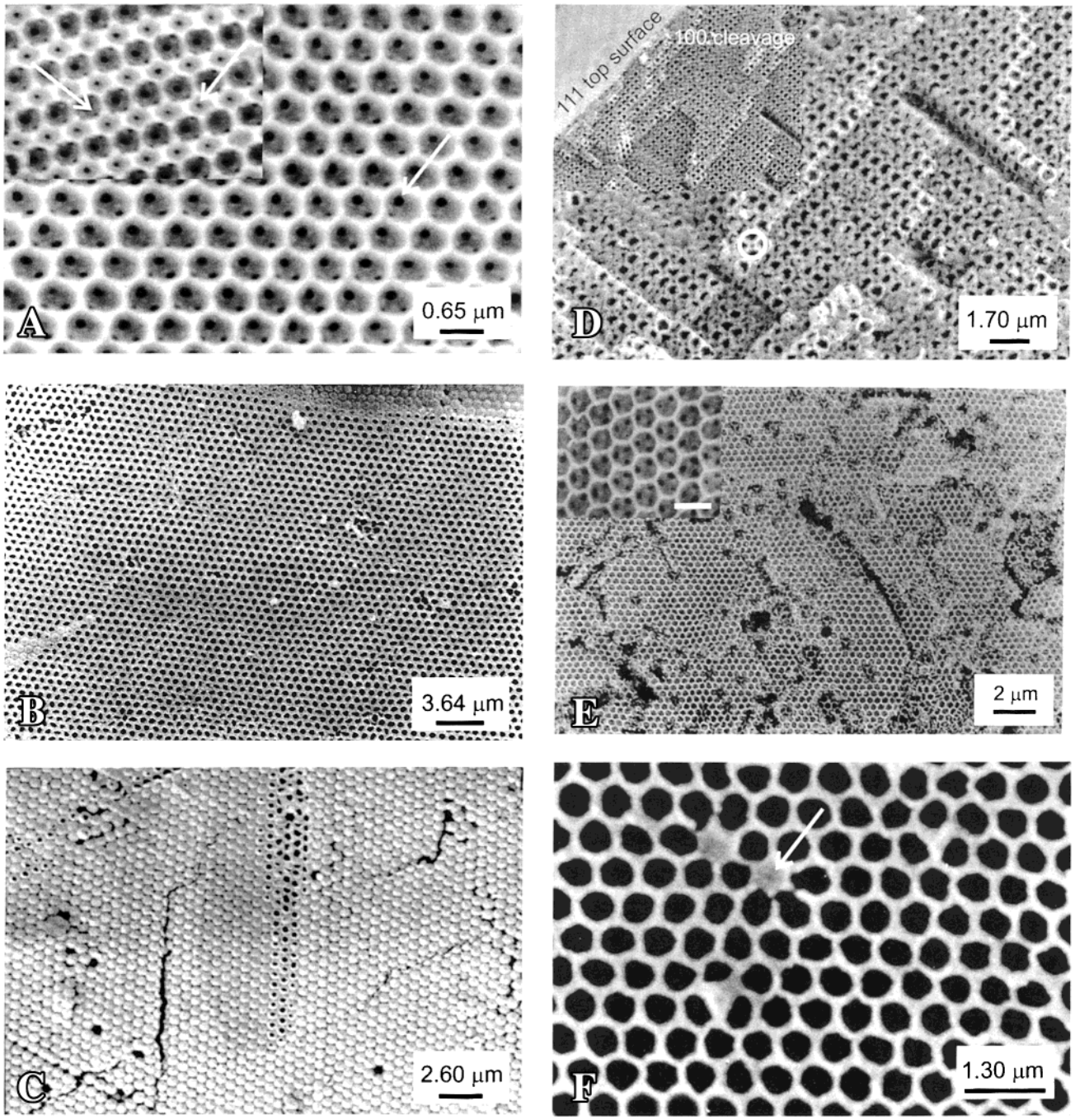

Figure 4. SEM images of air-sphere crystals made by using latex opals as template. Scale bars are indicated in each panel. (a) A nearly perfect hexagonal arrangement of macropores of radius 322 ± 3 nm that forms an fcc [111] surface plane. The dark spots are remnants of the contact points between nearest-neighbor spheres in the template that have developed into windows between the pores. Inset: rectangular arrangement of a single domain of macropores of the same sample. The rectangles have edge ratio 1 to $(2)^{1/2}$ and are a [110] cleavage plane. The smaller pores are from a layer at a more elevated height (toward the viewer), whereas the large pores are in a next layer that is deeper down. The arrows indicate windows that connect the air spheres to nearest neighbors in the next deeper layers. (b) Zoomed-out view of a single domain of 48 × 60 spheres in a different sample with $R = 325 \pm 3$ nm. The macropores show a variation of shapes, from circular to elongated, probably due to anisotropic crystallization or shrinkage of the TiO_2. (c) Single domain of 35 × 57 macropores (same sample as in (a)). The surfaces of most pores are closed and covered by titania, because the opal was not touching the glass wall of the capillary and the precursors could cover the whole sphere. Near the center, several open pores are visible. The dark vertical line at the lower left is a line defect (break). (d) Square arrangement of macropores of an inverse opal with $R = 300 \pm 3$ nm. The steps on this [100] plane are the result of the breakage of an inverse opal into two pieces. In the middle of each square of macropores, one small additional void is apparent, as highlighted by the white circle. These voids are the result of surface templating of the titania. Inset: zoomed-out image of the sample in Figure 4d. At the top left, a [111] surface plane is apparent. No vacancies appear in the [100] plane. (e) [111] arrangement of macropores in titania with radius 177 ± 2 nm. The sample was infiltrated only twice and is incompletely infiltrated. Many holes, which are single and multiple vacancies, are visible. The inset shows a close-up of a well-infiltrated part of the sample with macropores and interconnecting windows as dark spots. (f) Macropores with [111] surface plane, made with extra water (same sample as in (a)). The arrow indicates a pore that appears to be completely infiltrated with titania.

calcination, the uncovered areas are apparent as windows between the air spheres. While the presence of windows might be expected to decrease photonic crystal properties because the volume fraction of high-dielectric material is reduced, the windows rather enhance the widths of the photonic gaps. This is borne out by band structure calculations.[35,36] It also agrees with the experimental observations that titania inverse opals with windows have wider first-order stop gaps of about 14−15%[32,39,40] than titania inverse opals with closed shells, whose stop gaps are up to 10% wide.[33] It was well-known from theory that a three-dimensional connectivity of both high- and low-dielectric materials in a photonic crystal is favorable.[23,55]

We now turn to the deviations from most commonly observed structures in our inverse opals. Figure 4b shows a zoomed-out image of the surface of a different sample with $R = 304$ nm, that was made without added water. The domain pictured is a large single crystal similar to the one in ref 40 that measures 48 × 60 spheres, or 29 × 37 μm. A peculiar feature is seen on this surface; the shape of the openings of the macropores varies over the surface, varying from the usual circular shapes to elongated shapes. The distortion in the circular shape is tentatively attributed to anisotropic crystallization of the TiO_2 or to anisotropic shrinkage. Nevertheless, it is clear that the long-range crystalline order of the surface is not affected by this feature. In the section on SAXS, it is shown that the macropores have a very low size polydispersity. This suggests that the distortions occur only at the surface and hence hardly affect the photonic crystal properties of the bulk, other than adding some surface diffuse scattering.

Figure 4c shows an interesting feature that occurs on a surface of a macroporous crystal; instead of being "open", as in Figure 4a and as usually reported in the literature, nearly all the pores are totally covered with a shell of titania. A few macropores near the center of the SEM have partially open surfaces. Since such "closed" ordered pores have not been reported elsewhere, it is attributed to a characteristic of our sample synthesis, in particular the growth inside glass capillaries. We propose that closed macropores are related to incomplete wetting of the alkoxide on the glass wall of the capillary during the synthesis; if the opal spheres are close to the glass wall, the opal surface cannot be completely covered, resulting in surfaces as in Figure 4a. If there is some space between the opal and the glass wall due to shrinkage of the opal upon drying, the latex can be completely covered with the TPT/ethanol mixture, resulting in covered surfaces as in Figure 4c. We note that there is optically no noticeable difference between macropores with closed or open surfaces; both kinds reveal the same beautiful colored iridescence. Therefore, we do not consider closed air spheres as a defect. The surface in Figure 4c also reveals a small line defect (lower left) that we attribute to strain as a result of the shrinkage that occurs during the calcination. Nevertheless, the fissure is much smaller than the whole crystal domain. Thus, this SEM picture shows a large single domain of 35 × 57 spheres, or 22 × 35 μm.

Figure 4d shows the [100] plane of an inverse opal. This plane is obtained by breaking an inverse opal into two pieces. Thus, it shows the inner side of the inverse crystal. The top left part in the inset is a [111] top surface similar to the ones described above. The observation of a [100] plane is important crystallographic information, as it immediately rules out various close-packed hexagonal structures, such as hcp or random stacks of hexagonal planes that are often reported for colloidal crystals,[58] and confirms that our crystals are fcc. The crystal depicted is part of a single crystal of at least 39 × 39 μm with many steps on its cleavage surface. These steps are due to the cleavage. In this sample, no signs of incomplete filling (as in Figure 4e below) are visible. The main part of Figure 4d is a close-up of the same sample. We observed small additional openings between the air spheres that are arranged in a square grid, as highlighted by the white circle. Such interstitial voids were first noted in ref 11 and have also been observed elsewhere;[32] the voids are not infiltrated, since the precipitation of titania apparently starts from the surface of the colloidal spheres. The adherence of titania to polystyrene surfaces is clearly illustrated in the recent synthesis study of Jiang et al.[56] The result is that layers of titania cover the polystyrene template spheres. The octahedral interstitials remain open, because the channels between these interstitials become blocked by the precipitates from the TPT/ethanol precursor. This kind of filling is termed surface templating by Zakhidov et al.[16] If the precipitation would have started from the volume between the spheres, called volume templating,[16] small loose pieces of titania would be expected, but these are not observed. With methods such as infiltrating by electrochemical deposition,[19,57] the space between the spheres is filled. However, for photonic crystals, complete infiltration does not seem to be necessary[19] and the occurrence of voids appears to be favorable,[35] as with the windows mentioned above.

In Figure 4e, an incompletely filled crystal, which was infiltrated with the precursors only twice, is shown. The image reveals vacancies and some local distortions between well-ordered regions. The inset shows an enlargement of a regular well-filled part from the middle of the sample. Therefore, we propose that the vacancies are places where the precursors did not enter the interstitial space between the spheres in the template. Apparently, the infiltration proceeds inhomogeneously throughout the template. At each infiltration step, the TPT/ethanol mixture nucleates solid material in a small region. The successive infiltration steps are necessary to fill a large part of the template and form large domains as shown in parts a and b of Figure 4.

A titania sample made with extra water is illustrated in Figure 4f. This is a detailed view of 11 × 13 air spheres with an average radius of 326 nm. The peculiar feature is the appearance of solid pieces of material both inside the air spheres, as indicated by the arrow, and

(55) Economou, E. N.; Sigalas, M. M. *Phys. Rev. B* **1992**, *48*, 13434−13438.

(56) Jiang, P.; Bertone, J. F.; Colvin, V. L. *Science* **2001**, *291*, 453−457.

(57) Wijnhoven, J. E. G. J.; Zevenhuizen, S. J. M.; Hendriks, M.; Vanmaekelbergh, D.; Kelly, J. J.; Vos W. L. *Adv. Mater.* **2000**, *12*, 888−890.

(58) Vlasov, Y. A.; Astratov, V. N.; Baryshev, A. V.; Kaplyanskii, A. A.; Karimov, O. Z.; Limonov, M. F. *Phys. Rev. E* **2000**, *61*, 5784−5793.

between three spheres (lower left). These solid pieces appear as solid titania defects, although it cannot be excluded that they effectively are "caps" on top of the air spheres. If these features are indeed solid, this is exciting from a photonic crystal point of view, because they would serve as photonic defects that concentrate the light field in the high-dielectric material.[23] Such features were observed in at least four different samples but were never observed by us in the syntheses without added water. Similar features are apparent, but not discussed, in the recent work of Meng et al.[59]

(c) SAXS. (i) Diffraction Patterns. Figure 5 shows X-ray diffraction patterns at various orientations of an inverse opal made from spheres with radii of 439 nm. The intensities were corrected for the response of the CCD detector. The scales of the wave vector s in both the x- and y-direction are shown along with a scale bar for the intensities. The low-intensity (dark) feature extending from the center to the left is a shadow from the beam stop that protects the detector from the direct beam. The sharp Bragg peaks and the symmetric positioning of the peaks suggest that a single-crystal domain is irradiated by the X-ray beam. Indeed, we observed doubling or tripling of each peak or even concentric rings when the sample was translated, which meant that the X-ray beam then irradiated two, three, or many crystals. These observations confirm that the patterns in Figure 5 are the diffraction patterns of a large single crystal. Because the size of the crystal is of the order of the size of the X-ray beam, 0.3 × 0.6 mm in cross section, and the thickness is about 210 μm, we estimated this crystal domain to be at least 700 × 350 unit cells in cross section and 250 unit cells thick. We observed such large domains in several different inverse opal samples as well as in parent opal samples.

Many Bragg diffraction peaks are observed simultaneously in this monochromatic experiment, in contrast to X-ray diffraction of atomic single crystals. The reason is that the X-ray wavelength λ is much smaller than the typical lattice spacings d. Conversely, the radius $1/\lambda$ of the Ewald scattering sphere is much larger than the lengths $1/d$ of the reciprocal lattice vectors, see refs 49 and 37. Consequently, the Ewald sphere becomes a scattering plane that intersects many reciprocal lattice vectors simultaneously.

The upper pattern in Figure 5 was recorded at an angle of $\omega = -53°$. A square symmetry is apparent, which indicates that the pattern consists of reciprocal lattice vectors perpendicular to a cubic ⟨100⟩ crystal axis. Upon rotation to $\omega = 0°$, shown in the middle pattern, a hexagonal pattern appears that is perpendicular to a ⟨111⟩ axis. This is to be expected since colloids that form the template order themselves in hcp planes parallel to the capillary walls.[27,28] In the lower pattern at $\omega = 35°$, a rectangular pattern appears that is perpendicular to a ⟨110⟩ axis. All Bragg reflections in Figure 5 can be indexed with an fcc crystal structure with cubic lattice parameter $a = 861 \pm 12$ nm. From these results, the radii of close-packed macropores is derived as $R_{SAXS1} = a/(2(2^{1/2})) = 304 \pm 5$ nm; see Table 1. The observation of fcc crystals agrees with prior results on colloidal crystals made of polystyrene colloids,[27,28] which are the

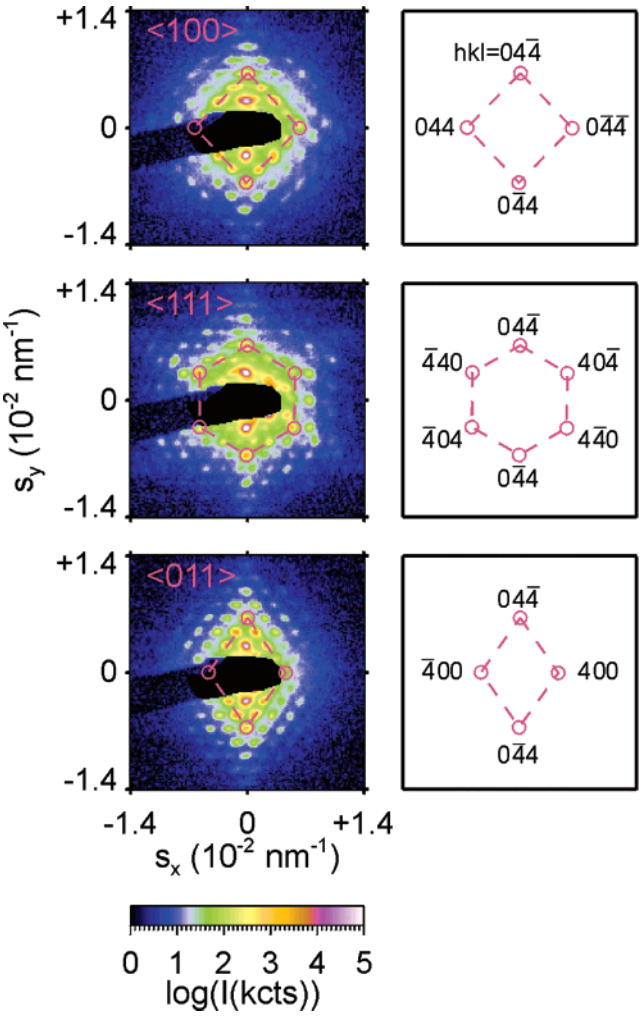

Figure 5. Small-angle X-ray diffraction patterns of a single crystal of air spheres in titania with cubic lattice parameter $a = 861 \pm 12$ nm. The logarithmic intensity scale is indicated at the bottom. The dark feature extending from center to left in each pattern is the shadow of the beam stop. The upper pattern indicated with the ⟨100⟩ axis was taken at $\omega = -53°$. Four reflections in a square arrangement from the $hkl = 044$ class are highlighted in the diffraction pattern and identified in the panel at the right. The middle pattern indicated with the ⟨111⟩ axis was taken at $\omega = 0°$. Six reflections in a hexagonal arrangement from the $hkl = 044$ class are highlighted in the diffraction pattern and identified in the panel at the right. The lower pattern indicated with the ⟨011⟩ axis was taken at $\omega = +35°$. Four reflections in an oblique arrangement from the $hkl = 044$ and 400 classes are highlighted in the diffraction pattern and identified in the panel at the right.

parent structures of the inverse opals. In a detailed analysis of such crystals, conservative upper bounds of <5 and <10 vol % could be placed on hcp and random stacks of hexagonal planes, respectively.[60] In inverse opals, we never obtained evidence for twinning or for other crystal structures with stacking faults along the c-axis such as random stacks of hexagonal planes. The latter has been reported for silica spheres; see, e.g., ref 58 and references therein. Also, we detected fcc crystals only in colloidal crystals made of silica spheres. We propose that we observed fcc crystals because our colloidal spheres, both polystyrene and silica, are usu-

(59) Meng, Q. B.; Gu, Z. Z.; Sato, O.; Fujishima, A. *Appl. Phys. Lett.* **2000**, *77*, 4313−4315.

(60) Megens, M.; Vos W. L. *Phys. Rev. Lett.* **2000**, *86*, 4855−4858.

ally charged; hence, they have a long-range interparticle interaction. The observation of fcc inverse opals is favorable from a photonic crystal perspective, since fcc inverse opals are predicted to develop photonic band gaps.[34,35]

To facilitate the indexing of the patterns, we highlighted several Bragg peaks in the diffraction patterns with red circles. The same circles are indicated in the empty panels on the right side with their Miller indices. For the ⟨100⟩ pattern, the four highlighted Bragg reflections are clockwise from top: $hkl = 04\bar{4}$, $0\bar{4}\bar{4}$, $0\bar{4}4$, and 044, with the last one being blocked by the beam stop. The peaks correspond to lattice spacings of d =152 nm. Given these Bragg reflections, others are easily indexed. For instance, on a line that connects the $04\bar{4}$ and $0\bar{4}\bar{4}$ peaks the ones that are between are $02\bar{4}$, $00\bar{4}$, and $0\bar{2}\bar{4}$. The two brightest Bragg reflections close to the beam stop are $hkl = 02\bar{2}$ at a wave vector of 0 nm^{-1} (0.4×10^{-2} nm^{-1}) and $hkl = 0\bar{2}2$ at a wave vector of 0 nm^{-1} (-0.4×10^{-2} nm^{-1}). These reflections correspond to large lattice spacings of d = 301 nm, more than 3000 times larger than the X-ray wavelength of 0.1 nm.

In the ⟨111⟩ pattern, we indicated the following reflections clockwise from the top: $hkl = 04\bar{4}$, $40\bar{4}$, $4\bar{4}0$, $0\bar{4}4$, $\bar{4}04$, and $\bar{4}40$. The reflections highlighted in the ⟨011⟩ pattern are $hkl = 04\bar{4}$, 400, $0\bar{4}4$, and $\bar{4}00$. The ω rotation axis is on the axis $s_x = 0$; therefore, the reflections on this axis do not change in the sequence of diffraction patterns. The crystallographic orientation of this sample is completely characterized. This has proven to be essential information for subsequent optical reflectivity experiments as described in ref 40. Such experiments were done in the horizontal plane, i.e., the $s_y = 0$ plane in Figure 5. With Brillouin zone indexing used in solid-state physics, the upper panel corresponds to the high symmetry point X, the middle one to the L-point, and the lower one to the K-point.

Reflections with larger Miller indices are also apparent in the diffraction patterns: there is clearly an $06\bar{6}$ reflection and even evidence for an $08\bar{8}$ reflection extending from the center of the pattern beyond the $04\bar{4}$ reflection. Similar results pertain in the opposite $0\bar{4}4$ direction. The large number of Bragg reflections observed, with Miller indices up to hkl = 880, indicates that the air spheres are highly ordered and are on average located close to their ideal lattice sites.[27,60] In the parent colloidal crystals, displacements less than 6% of the nearest-neighbor distance were observed for densities of less than 57 vol %.[60] The displacements further decreased as the density increased toward the close-packed limit of 74 vol % of opals.

Optically, the Bragg reflections with high Miller indices correspond to plane waves with high Miller indices; the observed reflections extend far beyond the second-order Bragg reflections where the photonic band gap of fcc crystals develops.[34,36,35]

(ii) Macropore Surface Roughness. Figure 6a shows a SAXS pattern as a function of scattering vector s, obtained from an inverse opal with a lattice parameter a = 480 ± 10 nm (circles). This pattern was obtained by azimuthally averaging two-dimensional SAXS patterns similar to those in Figure 5 about the beam center. At small scattering vectors, Bragg peaks are apparent in Figure 6a. With increasing scattering vector s, the peaks decay and the scattered intensity mainly provides information about the scattering units, that is, about the individual air spheres. It was seen that the intensity decreased as a power law of the scattering vector with an exponent $b = 3.40 \pm 0.08$. For all inverse opals, we observed similar power law behavior at scattering vectors larger than about 0.016 nm^{-1}, with exponents ranging from b = 3.28−3.5.

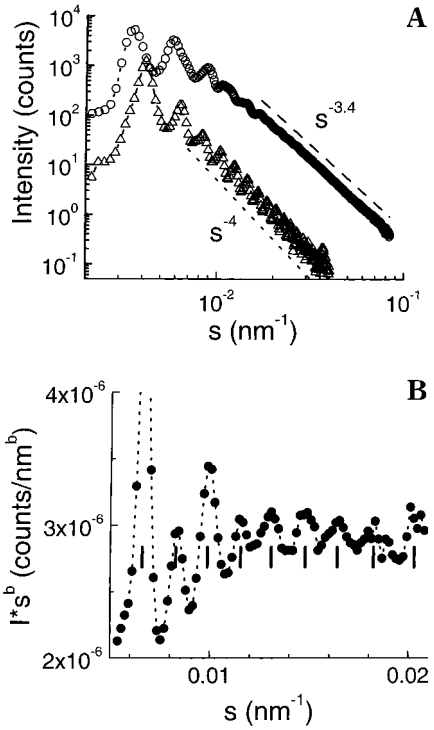

Figure 6. (a) X-ray diffracted intensity I as a function of scattering vector s on a log−log plot. The exponent b of the powerlaw $I \propto s^b$ is obtained from the slope of the curve at large s. The exponent is $b = 3.40 \pm 0.08$ for an inverse opal (with $R_{SAXS1} = 220 \pm 4$ nm, circles) and $b = 3.88 \pm 0.06$ for an opal ($R_{SAXS1} = 244 \pm 4$ nm, triangles). A slope of −3.4 is indicated by a long dashed line and the slope of −4 by a short dashed line. (b) X-ray diffracted intensity I multiplied by scattering vector s^b as a function of s (Porod plot). Fringes indicated by vertical marks are oscillations in the form factor of the macropores. The period 0.001 63(1) nm^{-1} corresponds to macropore radius R_{SAXS2} = 307 ± 1 nm. Observation of the 12th fringe at $s = 0.0203$ nm^{-1} indicates a small size polydispersity, $\Delta R/R$ < 3%.

The exponent of the scattered intensity vs the scattering vector provides information about the general shape of the scattering units. Solid particles with a sharp edge such as colloidal particles have an exponent $b = 4$,[45,51] as is illustrated in Figure 6a for a polystyrene opal with a lattice parameter a = 680 ± 10 nm (triangles). Our experiments revealed exponents between $3.88 < b < 4.14$ for dilute colloidal suspensions and for opals. Thus, we can exclude that the inverse opals consist of voids with sharp interfaces embedded in a solid backbone. It is also interesting to note that the observed exponent for the inverse opals is clearly not equal to 2. This excludes a structural model of air spheres surrounded by infinitesimally thin shells of solid material. The observed exponents of $3.28 < b < 3.5$ are consistent with a model of air spheres embedded in a homogeneous solid with a rough interface whose roughness is distributed with a power law, termed surface

fractal.[61,62] It seems to be a great challenge to characterize the size and statistics of such roughness by electron or atomic force microscopy; in a recent example of a macropore in gold (Figure 3f of Velev and Kaler[3]), roughness is apparent but has not been analyzed. The surface fractal dimension is equal to $D_s = 6 - b = 2.5-2.72$, similar to observations on inorganic gels and on porous rocks.[61,62] The minimum scattering vector 0.016 nm^{-1}, for which the power law behavior holds, sets a maximum length scale of 10 nm on the roughness of the surface (cf. ref 62, p 532−536). This value agrees with the typical size of the grains of titania of 20 nm extracted from the Scherrer broadening in wide-angle X-ray diffraction patterns.

It is proposed that the fractal roughness observed here could influence surface dependent properties such as catalysis by recently developed macroporous materials with zeolitic walls.[52] Since the relevant length scales are more than 10 times less than the wavelength of light, the roughness will contribute to a Rayleigh diffuse scattering,[41] but otherwise it seems unlikely that the surface roughness affects photonic crystal properties.

(iii) Form Factor and Size Polydispersity. Figure 6b shows the azimuthally integrated SAXS intensity multiplied with the scattering vector to the power b vs scattering vector, also known as a Porod plot.[45] The pattern reveals oscillations, indicated by tick marks, with a period of 0.001 63(1) nm^{-1} that are reminiscent of oscillations in the form factors of dilute colloidal spheres.[51] This period is expected to be the inverse of the radius R_{SAXS2} of the air spheres. We obtained $R_{SAXS2} = 307 \pm 1$ nm, which agrees very well with $R_{SAXS1} = 304 \pm 5$ nm from the lattice parameter and with $R_{SEM} = 325 \pm 5$ nm obtained from the SEM data; see Table 1. A detailed analysis revealed that the radii R_{SAXS2} are always slightly larger, up to a few percent, than the radii R_{SAXS1}. The radii R_{SAXS1} are obtained by assuming that the crystal consists of close-packed pores that touch at one point: the inner radius of the air spheres; hence, $R_{SAXS1} = a/(2(2^{1/2}))$. The radii R_{SAXS2} obtained from the form factor are an average of the inner radius of the pore (equal to R_{SAXS1}) and a larger radius that includes the thickness of a shell of titania around each air sphere (for an example, see Figure 2B in ref 11). Therefore, R_{SAXS2} is slightly larger than R_{SAXS1}.

The observation of a large number of oscillations in the Porod plot, up to a 12th at $s = 0.0203$ nm^{-1} in Figure 6b, indicates that the air spheres have a small size variation. Since the functional shape for the form factor of macropores as a function of s and orientation is a much more complex function than for spherical colloids, we estimate the size polydispersity $\Delta R/R$ to be <3% by comparison to a sample of silica colloids that revealed a similar number of fringes (Figure 3c of ref 51). To our knowledge, this is the first attempt to determine the size variation of macropores that profits from the statistical sampling in a scattering experiment. The small polydispersity means that the narrow size distribution of the original colloidal spheres in the template is retained in the air spheres. The size polydispersity is an important parameter for inverse opal photonic crystals. In recent work, Li and Zhang[38] calculated that photonic band gaps are only developed for well-ordered systems with $\Delta r/r < 5\%$. Thus, crystals made by the preparation method described in this paper fulfill this requirement. (There is a subtle difference in the size variations: our analysis assumes a Gaussian distribution of sizes, whereas Li and Zhang[38] assumed a square distribution.)

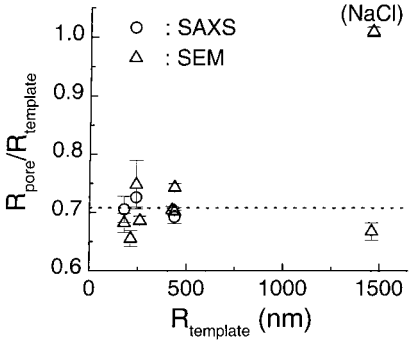

Figure 7. Radii of macropores in titania R_{pore} normalized to the radii of the colloidal particles in the opal templates $R_{template}$ as a function of $R_{template}$. The circles are obtained from the cubic lattice parameters a as $R_{SAXS1} = a/(8)^{1/2}$, and the triangles are obtained from R_{SEM}. The triangle near (1500 nm, 1.0) is a result for macropores in rocksalt.

(d) Radii of the Macropores and Shrinkage. The radii of the macropores that were obtained by SEM and by SAXS are listed in Table 1 in the sixth through the eighth columns. For ease of comparison, we have plotted in Figure 7 the ratio $R_{pore}/R_{template}$ of the radii of the macropores to the radii of the corresponding template spheres as a function of the radii of the template spheres $R_{template}$. The ratio is clearly <1, thus the air spheres in titania are much smaller than the colloids of the templates. The ratio $R_{pore}/R_{template}$ is constant as a function of the size of the spheres; no trend is apparent in the amount of shrinkage for the various sizes spheres used as templates. No influence of the volume fraction of TiO_2 was observed on the shrinkage, contrary to a previous suggestion.[19] Averaging all SEM data, we find a ratio $R_{pore}/R_{template} = 0.70 \pm 0.03$ in excellent agreement with the SAXS lattice parameter data: $R_{pore}/R_{template} = 0.71 \pm 0.02$. Thus, the inverse opals experience about 30% linear shrinkage, which agrees with earlier reports on ceramics.[14,62]

After the repeated filling cycles, the solid material between the spheres is not TiO_2 yet but a hydrolyzed TPT species that probably still contains many hydroxyl groups. The reaction from this species to crystalline TiO_2 proceeds at high temperatures where the latex template has already burned and thus does not prevent morphological changes. Since there is a considerable density difference between the precursors and TiO_2 (e.g., 1.03 g cm^{-3} for TPT and 3.9 g cm^{-3} for anatase), shrinkage is likely. Shrinkage does not happen if the filling material is in its final form before the template is removed, as is illustrated by our experiences on rocksalt (see Figure 11) or gold.[57] In the case of macropores in a backbone that is assembled from a gel of small particles of the same material, a shrinkage of 6% has been reported in the case of SiO_2 nanoparticles.[31] The small remnant shrinkage is perhaps due to the filling of the empty spaces between the nanoparticles.

(61) Auvray, L.; Auroy, P. *Neutron, X-ray, and Light Scattering*; Lindner, P., Zemb, Th., Eds.; Elsevier Science: Amsterdam, 1991.
(62) Brinker, C. J.; Scherer, G. W. *Sol−Gel Science*; Academic Press: San Diego, 1990.

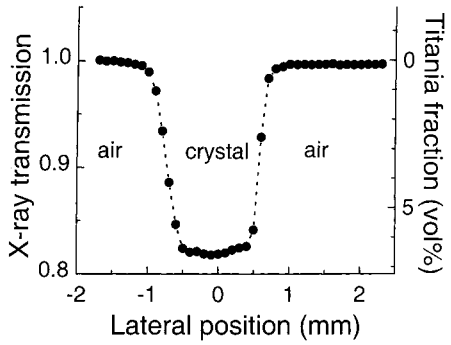

Figure 8. Transmission of X-rays through an inverse opal in titania ($R = 143$ nm) as a function of the sample position. The sample was scanned vertically (*z*-direction), the direction in which the beam size is about 0.3 mm. The width of the sample is about 1.3 mm.

(e) Volume Fraction of Titania. While a sample is being positioned in the X-ray beam for SAXS experiments, many alignment scans are performed. In such a scan, shown in Figure 8, the transmission of a macroporous sample taken out of the capillary is measured as a function of the sample position. The transmission is $T = 1$ if the sample is outside the X-ray beam and reduces to $T = 0.82$ if the sample is positioned in the beam. The nearly constant transmission from -0.5 to $+0.5$ mm indicates that the sample is wider than the X-ray beam. The measured profile is a convolution of the geometries of the sample and of the beam. This type of measurement can be used to calculate the density of the material using Lambert−Beer's law, $T = I / I_0 = \exp(-\mu t)$, since the fraction of X-ray radiation scattered out of the transmitted beam is negligible.[37,45] Here, I_0 is the intensity of the incident beam, I is the intensity transmitted by the sample, μ is the total linear absorption coefficient (in cm^{-1}), and t is the thickness (in cm) of the sample. The density can then be calculated from μ, since the absorption coefficients of the constituent elements are known.[63] The right-hand axis of Figure 8 gives the volume fraction scale. In the example shown, the inverse opal contains ($\varphi_{titania}$) 6.5 vol % of TiO_2.

The densities of opals, opals infiltrated with TPT, and titania inverse opals are listed in Table 1. We have observed $\varphi_{titania} = 5-11.7$ vol % TiO_2 for the inverse opals, which is lower than the maximum of 26 vol % at complete infiltration. The reduction is a consequence of the incomplete infiltration of the voids in the structure (Figure 4d) and of the windows between the air spheres (Figure 4a). It is observed that for our small-pore samples, $\varphi_{titania} = 5$ to 7.6 vol %, whereas for pores larger than 300 nm, $\varphi_{titania} = 8$ to 11.7 vol %. While this difference correlates with the observation on SEM images that the windows in small-pore samples are often relatively larger, we cannot exclude incomplete infiltration of the small-pore samples studied.

For opals, the densities of polystyrene listed in the table are moderately reliable for two reasons. First, polystyrene consists only of carbon and hydrogen which are light atoms that absorb X-rays only weakly. Consequently, the transmission is very close to unity, which leads to a very large error in the calculated volume fractions. Second, the linear absorption coefficients for carbon and hydrogen have low accuracy.[63] The volume fraction of infiltrated opals is calculated assuming that the measured absorption is caused only by TiO_2. While precursors of TiO_2, unreacted TPT, and the polystyrene latex are still present in the samples, all the C and H atoms present have much lower absorption coefficients than TiO_2 and are present in unknown amounts after several infiltration cycles. The values in the table should therefore be lower limits; indeed, they are below the values of the macroporous samples.

It can be calculated that infiltrating an opal once with a TPT/ethanol mixture can yield an average TiO_2 volume fraction of 1.0 vol %; thus, a maximum of 8 filling cycles would correspond to a density of 8 vol %. This is not at all at variance with observed TiO_2 densities up to 12 vol %, since we have seen above (Figure 4e) that TiO_2 does not nucleate homogeneously over the whole template. There are regions in the opal where a lot of TiO_2 is deposited, usually near the bottom of the capillary. Here, large well-filled inverse opals are formed.

In previous work (ref 11), $\varphi_{titania}$ was estimated from the average refractive index n_{avg} obtained from optical measurement of λ_{111} and from the lattice spacing obtained from SEM images. Since the tilt correction for the SEM images had not been taken into account, the radii of the macropores and hence the lattice spacing was underestimated. Therefore, n_{avg} and consequently $\varphi_{titania}$ were overestimated. Even the use of angle-resolved reflectivity data[32] does not safeguard against overestimating $\varphi_{titania}$ because the apparent angle-dependent λ_{111} is systematically modified by multiple Bragg diffraction.[40] We recommend that it is best to perform a measurement of the volume fraction of the backbone independent from optical and SEM experiments.

An interesting manner to estimate the amount of deposited material is by weighing the samples.[14] In this way, the whole sample including infiltrated and non-infiltrated parts is averaged. In contrast, by X-ray absorption, well-infiltrated samples are probed in situ.

(f) Optical Bragg Reflection and Refractive Index. Study of the optical Bragg reflections of inverse opals provides important information on how such photonic crystals modify the propagation of light; see, for instance, refs 11, 24, 36, 39, and 40. In particular, the optical (111) Bragg reflection at normal incidence probes the stop gap in the Γ-L direction in the Brillouin zone.[39] Figure 9 shows the center wavelengths λ_{111} of the (111) optical Bragg reflection vs the radius R of the macropores, determined from SEM and SAXS. The wavelength λ_{111} increases linearly with R, as expected from simple scaling considerations; therefore, crystals with $R \sim 148$ nm have a blue or green opalescence[11] and crystals with $R \sim 180$ nm appear red.[39] It is known experimentally that the slope of λ_{111} vs R is determined by the average refractive index of the crystal n_{avg}.[47] (The average refractive index n_{avg} is not to be confused with the refractive index $n_{titania}$ of the titania.[4]) The data up to $R = 180$ nm, a lower TiO_2 volume fraction, yield $n_{avg} = 1.153 \pm 0.007$, and all data together result in $n_{avg} = 1.186 \pm 0.014$ indicated by the dashed line in Figure 9. The average refractive index n_{avg} depends on the refractive indices n_{air} and $n_{titania}$ and the volume fraction

(63) *International Tables for X-ray Crystallography*; Kynoch Press: Birmingham, 1962.

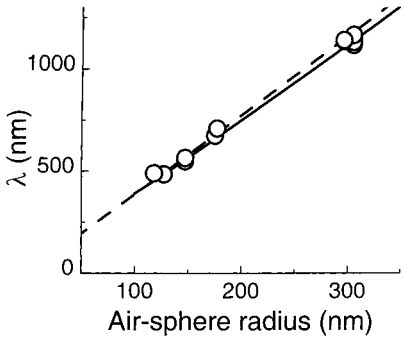

Figure 9. Wavelength of optical (111) Bragg diffraction peaks at normal incidence as a function of radius of the pores in the inverse opals. The dashed line is a model with the average refractive index $n_{avg} = 1.186 \pm 0.014$ as the only adjustable parameter. The solid curve is a simple Bragg model[45] with an average refractive index n_{avg}, which was calculated by assuming 10 vol % TiO_2 and taking into account the wavelength-dependent refractive index $n_{titania}$.[29]

$\varphi_{titania}$ through averaging relations such as the Maxwell-Garnett equations.[64,] Since $\varphi_{titania}$ is determined independently (see previous section) and $n_{air} = 1.00$, the refractive index $n_{titania}$ of the titania backbone can be obtained. From $n_{avg} = 1.153$ and $\varphi_{titania} = 6$ vol %, we obtain $n_{titania} = 2.9$, which is a high value for anatase, even considering that the results pertain to short wavelengths.[29] From $n_{avg} = 1.186 \pm 0.014$ and $\varphi_{titania} =$ 6 to 12 vol %, we obtain $n_{titania} = 2.7 \pm 0.4$. This value agrees well with the refractive index of bulk anatase in the visible range[29] but not with a reduced refractive index that has been observed for low-density titania made by sol−gel methods.[62,65] In Figure 9, we plotted the solid curve using the wavelength dependent $n_{titania}$[29] and assuming that $\varphi_{titania} = 10$ vol %. As expected, this curve agrees very well with the data, whereas curves for 5 or 15 vol % give lower and upper bounds to the data. Further confirmation that the titania in our samples closely matches bulk titania properties is the good agreement between multiple Bragg diffraction phenomena and band structures calculated with the bulk refractive index of titania.[36,40]

(g) Other Backbones: Rutile and Rocksalt. Titania has several solid polymorphs depending on the temperature to which it is heated. Rutile, the most stable phase, is formed at temperatures beyond 600 °C. Rutile is an interesting structure for photonic crystals because it has a ∼10% higher refractive index than anatase.[29] From wide-angle X-ray diffraction, it appears that the samples consist of anatase as expected because the samples are heated to 450 °C. We heated several samples to temperatures between 700 and 1000 °C to induce the phase transition from anatase to rutile. A SEM picture of a sample heated to 1000 °C is shown in Figure 10. From Raman spectroscopy, the backbone was identified as rutile. In contrast to the well-ordered structures shown above, no long-range order and no structure of air spheres are apparent in Figure 10. The heating of an already prepared anatase inverse opal to 1000 °C, the heating of an infiltrated opal to 1000 °C, or the varying of the heat all resulted in structures

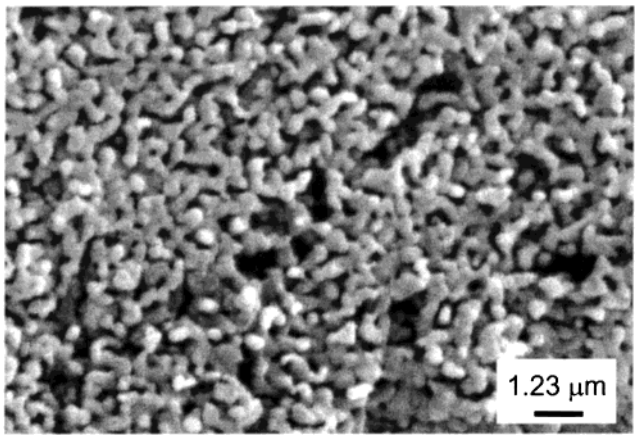

Figure 10. SEM image of an inverse opal in titania (template with $R = 426$ nm) heated to 1000 °C. The structure has no long-range order and no air spheres due to recrystallization of the titania.

similar to Figure 10. The heating of the opal to a temperature of 800 °C resulted in partial rutile and partial anatase samples as was determined by Raman spectroscopy. It was confirmed that the anatase parts were still well-ordered inverse opals, whereas the rutile regions were similar to the structure in Figure 10. The drastic change in morphology is attributed to the recrystallization of the TiO_2, which occurs long after the template has been removed earlier in the heating process. A successful method to making rutile inverse structures has been described by Imhof and Pine,[4] who templated titania from a sol−gel process with emulsions.

As an alternative to infiltrating the template with a precursor that reacts to form the solid backbone, we infiltrated templates with a saturated solution and allowed the solvent to evaporate while the solute was precipitated. We used a heated saturated solution of sodium chloride in water. Only one infiltration cycle of 3 h was needed to completely fill an opal template of polystyrene spheres with $R = 1480$ nm (Table 1). Apparently, the channels that connect the voids in the template are already blocked after one infiltration. After the latex was removed by heating, the structure shown in Figure 11 was observed. An ordered array of interconnected macropores is apparent in the rocksalt backbone. The radii of the pores is 1494 nm; hence, no shrinkage occurs within the error bars (see Figure 7). No shrinkage is expected because the rocksalt has already reached its final crystal structure and density upon evaporation of the solvent. Thus, this method is a promising method to make inverse opals.

Conclusions

We have described methods to fabricate macroporous crystals in a solid backbone with large domains. Our aim has been to achieve good-quality photonic crystals in a material with a large refractive index, which is TiO_2 in the present case. The techniques are simple, and the required materials are readily available. A high purity of the TiO_2 and concomitant low optical absorption are evident. While this is an important prerequisite for multiple light scattering typical of photonic band gap crystals, a high sample purity is also beneficial for materials science or chemical applications.

(64) Bohren, C. F.; Huffman, D. R. *Absorption and Scattering of Light by Small Particles*; Wiley: New York, 1983.

(65) Biswas, R.; Sigalas, M. M.; Subramania, G.; Soukoulis, C. M.; Ho, K. M. *Phys. Rev. B* **2000**, *61*, 4549−4553.

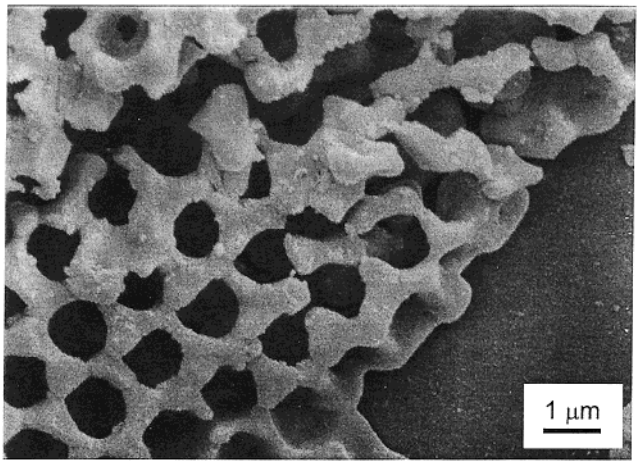

Figure 11. SEM image of a NaCl inverse opal, made by filling an opal with a heated saturated NaCl solution. The pores have a hexagonal arrangement and an average radius of 1494 ± 11 nm.

The opal templates are crystallized very slowly to get high-quality photonic crystals. The macropores at the surfaces of the crystals are ordered in hexagonal assemblies; square and rectangular arrangements are observed in cleavages. From SAXS diffraction patterns, the crystal structure is unambiguously determined as fcc, which is a favorable structure that will develop a photonic band gap.[34,36]

We have for the first time addressed important structural parameters that characterize the order of macroporous crystals: the size polydispersity of the macropores and the mean-squared displacements of the pores from the ideal lattice sites. Our crystals fulfill the stringent order requirements for band gap formation in inverse opals.[38] This is confirmed by the observation of complex optical behavior in the range of the second-order Bragg diffraction, which is the precursor to a photonic band gap.[36] While excellent order is not necessarily required for catalysis, chemical separation, or electrochemical applications, theoretical modeling may be facilitated, since the effects of fluctuations are reduced.

The macropores are close-packed and interconnected by windows. There are voids between the air spheres due to surface templation effects. While both features reduce the filling fraction of the solid backbone, their regular occurrence appears to enhance photonic crystal properties.[35] On smaller length scales, the TiO_2 backbone is composed of nanocrystalline grains. As a result, the surfaces of the macropores are rough, with a roughness that is fractally distributed. These features are likely to contribute to optical Rayleigh scattering, i.e., the whiteness of the crystals that occurs in addition to the opalescence. It is proposed that the nanoroughness is important for certain surface-specific applications such as in catalysis.

The SAXS experiments reveal patterns that are typical of single domains of more than 700 × 350 × 250 unit cells in size. On the other hand, electron microscopy reveals cracks on somewhat smaller scales. This situation is reminiscent of solid-state physics, where "Most real crystals consist of many slightly misaligned [single crystal] grains, separated by low-angle grain boundaries. The misalignment is little enough for X-ray diffraction to reveal sharp Bragg peaks ...".[49] Optically, cracks contribute to diffuse scattering and a reduction of maximum reflectivity. Low-angle grain boundaries also affect properties such as conductivity in electronic uses of macroporous materials, e.g., in electrochemistry or solar energy collection. The reduction of cracks that already appear in the template assembly is one of the main frontiers in the many uses of inverse opals.

While fcc inverse opals in titania will probably not reveal photonic band gaps, many efforts are being devoted to achieving macropores in materials with more elevated refractive indices or to the fabrication of structures with different crystal symmetries that may more easily allow band gap formation. In view of many exciting optical experiments, it is a safe conclusion that macroporous crystals have a bright future as three-dimensional photonic crystals.

Acknowledgment. We are grateful to Mischa Megens, Michiel Thijssen, and Henry van Driel for experimental help and pleasant discussions and Femius Koenderink for reading the manuscript. We thank Theyencheri Narayan and the staff of ESRF (Michael Hanfland) for expert help with the synchrotron experiments. Ad Lagendijk gave us generous encouragement and support. Denis Fenistein kindly pointed out scattering from rough surfaces. Wijnand Takkenberg and Bert Moleman helped with the SEM and the wide-angle X-ray diffraction, respectively. This work is part of the research program of the Stichting voor Fundamenteel Onderzoek der Materie (FOM), which is financially supported by the Nederlandse Organisatie voor Wetenschappelijk Onderzoek (NWO).

CM0111581